The American Journal of Pathology, Vol. 187, No. 6, June 2017

ELSEVIER

The American Journal of
PATHOLOGY
ajp.amjpathol.org

CELL INJURY, REPAIR, AGING, AND APOPTOSIS

Mechanisms of Retinal Damage after Ocular Alkali Burns

Eleftherios I. Paschalis,*†‡ Chengxin Zhou,*†‡ Fengyang Lei,*†‡ Nathan Scott,*†‡ Vassiliki Kapoulea,*†‡ Marie-Claude Robert,*†§ Demetrios Vavvas,*¶ Reza Dana,* James Chodosh,*‡ and Claes H. Dohlman*†

From the Boston Keratoprosthesis Laboratory,† Schepens Eye Research Institute, the Disruptive Technology Laboratory,‡ and the Angiogenesis Laboratory,¶ Massachusetts Eye and Ear, Department of Ophthalmology, Harvard Medical School, Boston, Massachusetts; and the Centre Hospitalier de l'Universite de Montreal,§ Hospital Notre-Dame, Montreal, Quebec, Canada*

Accepted for publication February 14, 2017.

Address correspondence to Eleftherios I. Paschalis, Ph.D., Department of Ophthalmology, Boston Keratoprosthesis Laboratory, Disruptive Technology Laboratory, Massachusetts Eye and Ear and Schepens Eye Research Institute, Harvard Medical School, Boston, Massachusetts 02114. E-mail: eleftherios_paschalis@meei.harvard.edu.

Alkali burns to the eye constitute a leading cause of worldwide blindness. In recent case series, corneal transplantation revealed unexpected damage to the retina and optic nerve in chemically burned eyes. We investigated the physical, biochemical, and immunological components of retinal injury after alkali burn and explored a novel neuroprotective regimen suitable for prompt administration in emergency departments. Thus, *in vivo* pH, oxygen, and oxidation reduction measurements were performed in the anterior and posterior segment of mouse and rabbit eyes using implantable microsensors. Tissue inflammation was assessed by immunohistochemistry and flow cytometry. The experiments confirmed that the retinal damage is not mediated by direct effect of the alkali, which is effectively buffered by the anterior segment. Rather, pH, oxygen, and oxidation reduction changes were restricted to the cornea and the anterior chamber, where they caused profound uveal inflammation and release of proinflammatory cytokines. The latter rapidly diffuse to the posterior segment, triggering retinal damage. Tumor necrosis factor-α was identified as a key proinflammatory mediator of retinal ganglion cell death. Blockade, by either monoclonal antibody or tumor necrosis factor receptor gene knockout, reduced inflammation and retinal ganglion cell loss. Intraocular pressure elevation was not observed in experimental alkali burns. These findings illuminate the mechanism by which alkali burns cause retinal damage and may have importance in designing therapies for retinal protection. *(Am J Pathol 2017, 187: 1327–1342; http://dx.doi.org/10.1016/j.ajpath.2017.02.005)*

Alkali burns may cause significant corneal scarring and blindness even if promptly treated.[1–4] Standard corneal transplantation can temporarily restore corneal clarity, but long-term results have been disappointing.[5] Burn-induced loss of limbal epithelial stem cells that regenerate corneal epithelium complicates surface healing.[6,7] Implantation of an artificial cornea can restore transparency. In many patients, the clear ocular media reveals the presence of optic nerve pallor and cupping, characteristic of retinal degeneration and severe glaucoma.[8] The mechanism of the damage to the posterior eye is not clear, but previous reports postulated that the alkali diffuses posteriorly and directly damages the retina.[9] Inflammatory intraocular pressure (IOP) elevation has also been implicated.[10] However, in a recent study on corneal alkali burns in rabbits (*in vivo*) and porcine eyes (*ex vivo*), direct pH determination performed in the vitreous revealed an unchanged, normal pH up to 6 hours after the burn. This casts doubt on the possibility of a direct effect of the alkali on the retina. In addition, tumor necrosis factor (TNF)-α expression was shown to acutely increase in the retinas of mice, followed by retinal ganglion cell (RGC) apoptosis 24 hours after the burn.[11] This

Supported by the Boston Keratoprosthesis Research Fund (E.I.P., C.Z., F.L., N.S., V.K., M.C.R., J.C., C.H.D.), Massachusetts Eye and Ear, the Eleanor and Miles Shore Fund (E.I.P.), the Massachusetts Lions Eye Research Fund (E.I.P.), a Research to Prevent Blindness (New York, NY) unrestricted grant (J.C.), and NIH National Eye Institute core grant P30EY003790.

E.I.P. and C.Z. contributed equally to this work.

Disclosures: None declared.

http://dx.doi.org/10.1016/j.ajpath.2017.02.005

suggests that the damage to the retina may be mediated by immunological processes, such inflammatory cytokines, rather than by direct pH change. These findings also raise the possibility of using targeted immunomodulatory therapy, such as antibody against TNF-α, for neuroprotection. Indeed, antibody against TNF-α given soon after burn was shown to provide significant protection to both the cornea and retina.[11] The promise of neuroprotection in human eyes after alkali burn prompted the present study. The goal of this study is to elucidate the biophysical and biological processes that lead to retina damage after alkali trauma and to explore the protective role of targeted immunomodulation with an anti−TNF-α agent as a novel adjunct therapy.

Materials and Methods

Mouse Model of Alkali Burn

All animal-based procedures were performed in accordance with the Association for Research in Vision and Ophthalmology Statement for the Use of Animals in Ophthalmic and Vision Research and the NIH *Guide for the Care and Use of Laboratory Animals*.[12] This study was approved by the Animal Care Committee of the Massachusetts Eye and Ear Infirmary. C57BL/6 and TNFRSF1A1B knockout mice were obtained from the Jackson Laboratory (Bar Harbor, ME). Mice between the ages of 6 and 12 weeks were used for this study. This model of alkali chemical burn is based on our previous study.[11] In brief, mice were anesthetized using 60 mg/kg ketamine and 6 mg/kg xylazine, and deep anesthesia was confirmed by a toe pinch test. Proparacaine hydrocloride USP 0.5% (Bausch and Lomb, Tampa, FL) eye drop was applied to the cornea for 1 minute and carefully dried with a Weck-Cel (Beaver Visitec International, Inc., Waltham, MA). A 2-mm-diameter filter paper was soaked into 1 mol/L sodium hydroxide solution for 10 seconds, dried from excess sodium hydroxide by a single touch on a paper towel, and applied onto the mouse cornea for 20 seconds. Complete adherence of the filter paper on the corneal surface was ensured by gentle push of the perimeter using forceps. After the filter paper was removed, prompt irrigation with sterile saline for 10 seconds was applied using a 50-mL syringe with a 25-gauge needle. The mouse was then placed on a heating pad, positioned laterally, and irrigated for another 15 minutes at low pressure using sterile saline. Buprenorphine hydrochloride (0.05 mg/kg; Buprenex Injectable; Reckitt Benckiser Healthcare Ltd, Hull, UK) was administered s.c. for pain management. A single drop of topical Polytrim antibiotic was administered after the irrigation (polymyxin B/trimethoprim; Bausch & Lomb Inc., Bridgewater, NJ). Mice were kept on a heating pad until fully awake.

Rabbit Model of Alkali Burn

New Zealand white rabbits, weighing 4 to 5 kg, were obtained from Charles River (Woburn, MA). Rabbits were placed on a heating pad, and anesthesia was administered using i.m. ketamine, 20 mg/kg, followed by i.p. injection of urethane, 1300 mg/kg (Sigma Aldrich, St. Louis, MO) diluted in 2-mL sterile water for injection.[13] Additional administration of urethane, 400 mg/kg, was provided every 5 hours to maintain anesthesia for 24 hours. Heart rate and temperature were continuously monitored. Alkali burn to the cornea was performed by placing an 8-mm trephine on the corneal surface and filling the trephine with 1 mL 2 mol/L sodium hydroxide for 40 seconds. The alkali was carefully absorbed from inside the trephine using a Weck-cel sponge, and the trephine was filled with 3 mL of sterile saline, which was then aspirated. The eye was then irrigated with saline solution for 20 seconds, followed by slow irrigation for 15 minutes, as described above. At the end of the experiment, an epidermal fentanyl patch was placed (12 μg/hour) for 3 days to reduce discomfort. Rabbits received twice-daily topical antibiotic ointment (erythromycin). Rabbits were euthanized at the completion of the experiment with 40 mg/kg ketamine and 10 mg/kg xylazine, followed by 100 mg/kg Fatal Plus IV injection (sodium pentobarbital).

pH, Oxygen, and Oxidation-Reduction Measurements

In vivo pH measurements were performed using two different pH probes: fiberoptic pH-1-micro with an outer diameter of 140 μm (PreSens, Regensburg, Germany) and microelectrode pH-50 with an outer diameter of 50 μm (Unisense, Aarhus, Denmark). Two different probes were used to validate the results. Briefly, the fiberoptic pH technology is based on dual-lifetime referencing technique. A fiberoptic probe is inserted in the eye and a coupled photo-emitting diode performs simultaneous excitation of a pair of luminophores, one reporting the pH and the other acting as reference.[14] The phase difference between the two excitations represents the pH of the sample and is independent of light intensity or wavelength interference. The probe has a linear response time of approximately 30 seconds at a pH range between 5.5 and 8.5 at 5°C to 50°C. At neutral pH, the probe has resolution ±0.001, accuracy ±0.05, and drift <0.05. The electrode pH sensor is based on selective diffusion of protons through pH-sensitive glass, and measures the potentials between the electrolyte and a reference electrode. The response time of the electrode is <10 seconds in the pH range 7 to 14, with resolution of 0.1 and linear response from 2 to 10 pH units from −10°C to 90°C. The sensors were precalibrated at pH 5, 7, and 10 before implantation, and the linear regression was calculated with $R^2 > 0.98$ in all cases.

In vivo oxygen measurements were performed using a 50-μm diameter glass-electrode oxygen sensor (Unisense, Aarhus, Denmark). The oxygen probe measures the diffusion of oxygen through a silicone membrane to an oxygen-reducing cathode. The reducing cathode is polarized against an internal silver/silver chloride anode, and the potential difference between the anode and cathode represents the oxygen partial pressure. The probe has linear response

between 0 and 1 Atm pO_2, with negligible oxygen consumption (10 to 16 mol/second) and response time <1 second. Before implantation, the probe was thoroughly prepolarized with −0.8 V for 24 hours and calibrated at maximum oxygen saturation (0.9% saline at 37°C with air agitation), and zero oxygen (2% sodium ascorbate in 0.1 mol/L sodium hydroxide solution). The probe was connected to a portable computer and measurements were acquired at 1 Hz (Nyquist-Shannon sampling theorem).

In vivo oxidation reduction (redox) measurements were performed using a 50-μm-diameter platinum glass-electrode redox sensor (Unisense, Aarhus, Denmark). An open-ended silver-silver chloride reference electrode was used. Briefly, redox electrode sensors measure the electric potential relative to the reference electrode, which shows the tendency of the solution to release (oxidation) or take up (reduction) electrons. Both electrodes were connected to a high-impedance millivolt meter and calibrated in a 4 and 7 pH/quinhydrone buffer (equal molarity mixture of hydrochinone and quinone). Measurements were acquired by a computer. The sensor can detect electric potential changes of 0.1 mV and has a response time <10 seconds.

Anterior Chamber pH, Oxygen, and Redox Measurements

Mice

Anesthetized mice were mounted in a stereotaxic frame (39463001; Leica, Buffalo Grove, IL) with Cunningham mouse adaptor (39462950; Leica). The head was immobilized, and a custom-made glass beveled needle (approximately 10 μm in diameter) was used to perform a narrow, self-sealing tunnel in the temporal region of the cornea, adjacent to the limbus. Before the insertion of the fine needle tip, it was marked with surgical dye (Accu-line Products Inc., Hyannis, MA) to guide the insertion of the sensor probe into the anterior chamber. Measurements were acquired at a sampling frequency of 60 Hz and stored in a portable computer. Afterward, the mice were euthanized by cervical dislocation.

Rabbits

Sensors were implanted in the anterior chamber of the eye of anesthetized rabbits through a temporal clear corneal tunnel, adjacent to the limbus, as described in the mice. Corneal burn was performed as described above, and measurements were acquired and stored in a portable computer at a sampling frequency of 60 Hz. Rabbits were euthanized by pentobarbital, 10 mg/kg (Fatal Plus) IV injection.

Vitreous pH, Oxygen, and Redox Measurements

Prolonged anesthesia in rabbits (>24 hours) was achieved with urethane i.p. injection. The upper lid was excised to expose the posterior segment of the globe, and the conjunctiva was surgically dissected to reveal the sclera. A full-thickness scleral tunnel was generated using a custom-made beveled glass needle (approximately 10 μm in diameter) that was marked with dye (Accu-line Products Inc.). The probes were introduced into the vitreous via the tunnel, and measurements were performed and logged in a computer. The probes were introduced into the vitreous cavity via the tunnel, and pH, oxygen, and redox measurements were performed and logged in a computer.

Suprachoroidal Measurements

The sensors were inserted into the suprachoroidal space through a small scleral incision 4 mm posterior to the limbus, and advanced posteriorly close to the optic nerve. A stereotaxic device (Leica 39463001) was used to control the position of the probe. Alkali burn was performed as described above, and measurements were performed every 20 seconds for 25 hours. A temperature probe, inserted into the rectum of the rabbit, was used to monitor body temperature. Anesthetized rabbits were euthanized after 25 hours.

IOP Measurements

Intraocular pressure measurements were performed in anesthetized rabbits and mice using a custom-made intracameral pressure transducer connected to a 33-gauge needle. The device was designed using a differential microelectromechanical pressure sensor 40 PC (Honeywell, Freeport, IL) connected to a 14-bit, 48 kilo samples per second data acquisition NI USB-6009 (National Instruments, Austin, TX), controlled by a proprietary software algorithm operating in Labview 2011 (National Instruments) environment. A special algorithm was designed to compensate for minute aqueous humor volume displacement during *in vivo* pressure measurements in mice. The device was assembled using microfluidic components (IDEX Health & Science, Oak Harbor, WA) with minimum dead volume. Before measurements, the remaining dead volume of the syringe was prefilled with sterile water, thus minimizing air compressibility only within the microelectromechanical cavity, which was compensated by the software algorithm. To perform measurements, the needle was inserted into the anterior chamber of the eye through a temporal clear corneal puncture, adjacent to the limbus, and the needle was advanced approximately 500 μm toward the center of the chamber. The contralateral eye served as internal control, and naive eyes served as physiological pressure reference.

Systemic Administration of Infliximab in Rabbits after Corneal Alkali Burn

Infliximab (Remicade) lyophilized powder was reconstituted to final concentration of 10 mg/kg of Remicade using 10 mL of 0.9% sodium chloride injection, USP. A 26-gauge butterfly catheter was inserted and secured with tape in the marginal ear vein, and the drug was slowly infused over 60 minutes, starting immediately after ocular irrigation (15 minutes).

Tissue Preparation for Immunohistochemistry

After alkali burn, eyes were enucleated at indicated time points and processed using OCT (Tissue Tek; Sakura, Leiden, the Netherlands) compound. Multiple sagittal sections of approximately 10 μm in thickness were obtained from the center and the periphery of the globe. Sectioned tissues were transferred to positive charged glass slides Superfrost Plus 75 × 25 mm, 1 mm thickness (VWR, Radnor, PA) and stored at −80°C for further processing.

Tissue Preparation for Flat Mount Imaging

After alkali burn, eyes were enucleated at indicated time points and fixed in 4% paraformaldehyde solution for 1 hour at 4°C. The cornea and retina tissue were carefully isolated using microsurgical techniques and washed three times for 5 minutes in phosphate-buffered saline solution (PBS) at 4°C. The tissues were then blocked using 5% bovine serum albumin and permeabilized using 0.3% Triton-X for 1 hour at 4°C. The specific antibody was added in blocking solution, incubated overnight at 4°C, and then washed three times for 10 minutes with 0.1% Triton-X in PBS. Tissues were transferred from the tube to positive charged glass slides Superfrost Plus 75 × 25 mm, 1 mm thickness using a wide pipette tip with the concave face upwards. Four relaxing incisions from the center to the periphery were made to generate four flat tissue quadrants. VECTRASHIELD mounting medium (H-1000; Vector Laboratories, Burlingame, CA) was placed over the tissue, followed by a coverslip.

TUNEL Labeling and Quantitation of DNA Fragmentation

After alkali burn, eyes were enucleated and cryosectioned. Terminal deoxynucleotidyl transferase-mediated dUTP nick-end labeling (TUNEL) labeling was performed using a Roche TUNEL kit (12156792910; Roche, Basel, Switzerland), as previously reported.[15] Mounting medium with DAPI (UltraCruz; sc-24941; Santa Cruz Biotechnology, Dallas, TX) was placed over the tissue, followed by a coverslip. Images were taken with an epifluorescent microscope (Zeiss Axio Imager M2; Zeiss, Oberkochen, Germany), using the tile technique. DAPI signal (blue) was overlayed with Texas red ($TUNEL^+$ cells) and quantified using ImageJ software version 1.43 or above (NIH, Bethesda, MD; *http://imagej.nih.gov/ij*) to measure the number of $TUNEL^+$ cells overlapping with DAPI in the areas of interest. All experiments were performed in triplicate.

Immunolocalization of TNF-α, Cleaved Caspase-3, β3-Tubulin, and Brn3a Protein

After alkali burn, eyes were enucleated at indicated time points and processed for frozen section, as described above. Sectioned tissues were fixated on the glass slides using 4% paraformaldehyde for 15 minutes at room temperature. The slides were then washed three times for 5 minutes in PBS and dried for paraffin boundary marking using paraffin pen.

TNF-α

Tissues were blocked with 5% bovine serum albumin (BSA) and incubated at 4°C overnight using 1:100 dilution of monoclonal anti-mouse fluorescein isothiocyanate conjugated antibody (NBP1-51502; Novus Biologicals, Littleton, CO). Tissues were washed three times for 5 minutes in PBS at room temperature and mounted using either VECTASHIELD or mounting medium with DAPI (UltraCruz; sc-24941; Santa Cruz Biotechnology), and covered with a coverslip.

Cleaved Caspase-3

Tissues were blocked with 5% BSA in PBS + 0.1 Tween-20 for 30 minutes at room temperature. Overnight incubation at 4°C was performed using rabbit monoclonal cleaved caspase-3 primary antibody (9664; Cell Signaling, Danvers, MA) at 1:300 dilution. Tissues were washed three times for 5 minutes in PBS, followed by incubation with preabsorbed goat anti-rabbit secondary antibody (DyLight 488; ab96895; Abcam, Cambridge, MA) at room temperature for 1 hour. Tissues were washed three times for 5 minutes in PBS at room temperature and mounted using medium with DAPI (UltraCruz) and covered using a coverslip.

Brn3a

Tissues were blocked with 5% BSA in PBS + 0.1 Tween-20 for 30 minutes at room temperature. Incubation at 4°C for 3 days was performed using goat polyclonal Brn3a (C-20) primary antibody (sc-31984Santa Cruz Biotechnology Inc.) at 1:50 dilution. Tissues were washed three times for 5 minutes in PBS, followed by donkey anti-goat secondary antibody (Alexa Fluor 488; ab150129; Abcam) incubation at room temperature for 1 hour. Tissues were washed three times for 5 minutes in PBS at room temperature, mounted using either VECTASHIELD or mounting medium with DAPI (UltraCruz), and covered using a coverslip.

β3-Tubulin

Tissues were blocked with 5% BSA in PBS + 0.1 Tween-20 for 30 minutes at room temperature. Overnight incubation at 4°C was performed using conjugated mouse monoclonal antibody (NL557; R&D Systems, Minneapolis, MN) at 1:100 dilution. Tissues were washed three times for 5 minutes in PBS at room temperature, mounted using either VECTASHIELD or mounting medium with DAPI (UltraCruz), and covered using a coverslip.

Paraphenylenediamine Staining

Optic nerve axon degeneration was evaluated in explanted rabbit eyes using paraphenylenediamine staining. Optic

nerves were dissected from the explanted eyes, fixed in Karnovsky fixative solution for 24 hours at 4°C, then processed and embedded in acrylic resin. Cross sections (1 μm thick) were obtained and stained with 1% paraphenylenediamine in absolute methanol. Each section was mounted onto glass slides and imaged with a bright field microscope (Nikon eclipse E800 DIC; Tokyo, Japan) using a 100× objective lens. Tile images of the whole nerve section were produced, and axon degeneration was analyzed using ImageJ software, according to previous protocols.[16–18]

Western Blot for Cleaved Caspase-3, TNF-α, and Endonuclease G

After alkali burn, eyes were enucleated and fresh retinas were dissected under a surgical microscope. Harvested tissues were placed in cryovials, frozen in liquid nitrogen, and stored at −80°C for further processing. When all tissue samples were collected, frozen tissues were suspended in buffer mixture of protease/phosphatase inhibitors and homogenized using a rotating cone. Samples were centrifuged at 11 × *g* for 15 minutes, and supernatant was collected and recentrifuged. A BSA assay was performed to quantify protein concentration, and all samples were normalized to 30 μg/mL using SDS buffer. Gels were prepared using acrylamide agarose 10% or purchased from Bio-Rad Laboratories (Hercules, CA). Cellulose transfer membrane was used to transfer the proteins from the gel to the methyl cellulose paper, followed by primary and secondary antibody staining.

Quantification of TNF-α Expression Using Immunohistochemistry

TNF-α expression was quantified using ImageJ software on whole eye tissue cross sections stained with DAPI and anti−TNF-α monoclonal antibody. Different time points were selected for analysis. For each time point, three different tissue sections from three different mice ($n = 3$) were used. The area of interest (cornea or retina) was marked using the freehand selection tool from ImageJ software and according to DAPI boundaries. The enclosed area was measured (mm^2), and the image was decomposed to red, green, and blue channels. The green channel that demonstrated expression of green fluorescent protein of TNF-α antibody was selected and converted to binary, and the positive pixels (bright pixels) were quantified by the ImageJ software. The outcome was normalized according to the total sampled area, and the resulting number was plotted.

Quantification of TUNEL$^+$ Cells Using Immunohistochemistry

Quantification of retinal TUNEL$^+$ cells was performed on whole eye tissue cross sections stained with DAPI and TUNEL assay using ImageJ software. Different retinal layers were quantified (ganglion cell layer; inner nuclear/plexiform layer; outer nuclear/plexiform layer). For each layer, two different tissue sections from three different mice ($n = 3$) were used. For each retinal layer, the percentage of TUNEL expression was calculated as the ratio of TUNEL/DAPI (area %) using particle analysis of ImageJ software. Data were presented as means ± SD.

Enzyme-Linked Immunosorbent Assay for Measuring TNF Receptor Protein Expression in Different Ocular Tissues

After burn, eyes were enucleated at indicated time points. Under the surgical dissecting microscope, the cornea, iris, lens, retina, and scleral tissues of each eye were isolated and placed in separate vials containing tissue lysis and protease inhibitor buffer. The tissues were homogenized using ultrasonication. The vials were maintained in ice for temperature control. Vials were centrifuged, and the supernatant was collected and stored at −20°C for further processing. TNF-R1 and TNF-R2 protein levels were quantified using enzyme-linked immunosorbent assay (R&D Systems), as described by the manufacturer.

Quantitative Real-Time RT-PCR for Measuring Proinflammatory Cytokine Expression in Cornea and Retina

After alkali burn, eyes were harvested at indicated time points. Corneal and retinal tissues were surgically dissected, placed in cryovials, and rapidly frozen in liquid nitrogen. RNA isolation was performed using Uneasy mini kit (74106; Qiagen, Valencia, CA) for retinas and Direct-zol RNA MiniPrep (R2052; Zymo Research Corp., Irvine, CA) for corneas. RNA quantification was performed using a nanodrop spectrophotometer (Nanodrop 2000; Thermo Scientific, Waltham, MA), and each sample was normalized before cDNA synthesis. cDNA synthesis was performed using superscript III (18080-044; Invitrogen, Carlsbad, CA). One microliter of cDNA was used in each real-time PCR. TaqMan primers were used to assess the expression levels of the following genes: *TNFA* (Mm99999068_m1; Life Technologies, Woburn, MA), *TNFR1* (Mm01182929_m1; Life Technologies), *TNFR2* (Mm00441889_m1; Life Technologies), *FAS* (Mm01204974_m1; Life Technologies), *FASLG* (Mm00438864_m1; Life Technologies), *IL1B* (MmMm00434228_m; Life Technologies), *INFG* (Mm01168134_m1; Life Technologies), and *MMP9* (Mm00442991_m1; Life Technologies). Each sample was run in triplicate, and three samples were used at each time point. The average cycle threshold (C_T) value was used in the analysis. C_T values were normalized using β-actin probe, and ranges were normalized based on naive control tissue. $\Delta\Delta C_T$ algorithm was used to compare mRNA levels.

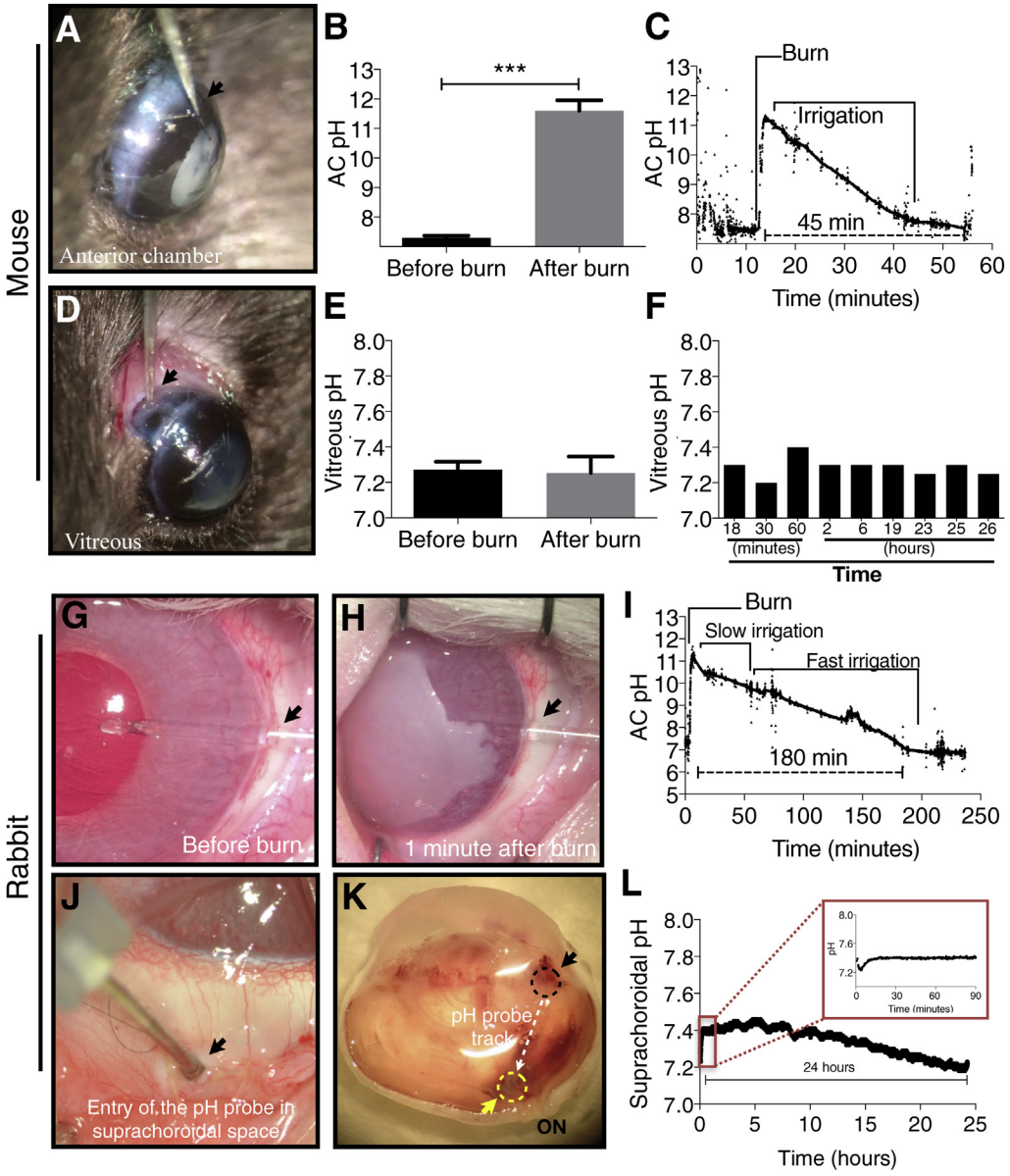

Figure 1 *In vivo* pH measurements in mice and rabbits after ocular alkali burn. **A**–**C:** The pH in the anterior chamber (AC) in mice was measured using an implantable probe. Corneal alkali burn causes rapid pH elevation of the aqueous humor (AH) from 7.4 to 11.4 within 40 seconds, followed by gradual normalization within 45 minutes. **D**–**F:** No significant pH change is noted in the vitreous within the first 24 hours after the burn, measured in consecutive mice at different time points. **F:** Each time point represents the average of repeated measurements of one mouse. **G**–**I:** The pH in the AC in rabbits was measured using two different implantable pH sensors (fiberoptic and electrode). Corneal alkali burn causes pH elevation in rabbit AH from 7.4 to 11.4 within 60 seconds, followed by a gradual normalization to pH 7.3 within the following 180 minutes, and stabilized at 6.9 between 180 and 230 minutes. **J** and **K:** Posterior segment (suprachoroidal) pH measurements were performed in anesthetized rabbits for 26 hours by implanting a pH probe in the suprachoroidal space near the optic nerve via a sclera tunnel. **L:** No pH elevation was measured in the suprachoroidal space 26 hours after the burn. **L:** A nonsignificant pH reduction is observed over time, which is attributed to tissue changes from the surgical trauma. **A**, **D**, **G**, **H**, **J**, and **K: Black arrowheads** show the entry point of the implantable probe in the eye. **K: Black dashed circle** shows the entry point of the probe in the suprachoroidal space. The **white dashed arrow** shows the path of implantation of the probe through the suprachoroidal space. The **yellow arrowhead** and the **yellow dashed circle** show the resting location of the tip of the probe during measurements. The tip was placed adjacent to the optic nerve (ON) via a suprachoroidal tunnel. $n = 10$ (**A**–**C**); $n = 9$ (**D**–**F**). $^{***}P < 0.001$.

Assessment of Immune Cell Activation/Infiltration in the Cornea and Retina by Flow Cytometry

Eyes were harvested at indicated time points. Corneas and retinas were isolated and processed for flow cytometry using collagenase type I and papain dissociation system (Worthington, Lakewood, NJ). Thy1.1-PE antibody (BioLegend, San Diego, CA) was used to identify RGCs, whereas immune cell activation was assessed using antibodies against CD45 and major histocompatibility complex (MHC)-II. Cells were analyzed on a BD LSR II cytometer (BD Biosciences, San Jose, CA) using FlowJo software version 10.2 (Tree Star, Ashland, OR).

Figure 2 Inflammatory response of the iris/ciliary body and retina after ocular alkali burn. **A:** Q1 to 3 represents the three quadrants of the flow cytometry data (Q1, $Ly6G^+/Ly6C^-$; Q2, $Ly6G^+/Ly6C^+$; and Q3, $Ly6G^-/Ly6C^+$ cell populations). Each quadrant was subanalyzed for CD11b and MHC-II expression. Corneal alkali burn causes increased numbers of $CD45^+$ cells in the iris and ciliary body. Most of these cells are positive for $Ly6C^+$ and $Ly6G^+$ markers and express MHC-II (Q1 to 3). Another two $CD45^+$ cell populations are present in the iris of burned eyes, the $Ly6G^+$ MHC-II^- and $Ly6C^+$ MHC-II^{lo}. **B:** Control iris/ciliary body shows a low frequency of $CD45^+$ cells, all of which are $Ly6G^-$ MHC-II^-. Corneal alkali burn causes robust up-regulation of TNF-α, IL-1β, TNF-R1 and R2, Fas, and MMP9 mRNA in the iris and ciliary body (**C**) and up-regulation of TNF-α, IL-1β, and INFγ mRNA in the retina (**D**). $^*P < 0.05$, $^{***}P < 0.001$, and $^{****}P < 0.0001$ compared to naive controls. FSC, forward scatter.

TNF-α Blockade

TNF-α blockade was performed using infliximab, a Federal Drug Administration–approved chimeric (mouse-human) monoclonal antibody (Remicade; Janssen Biotech, Inc., Horsham, PA). Administration in mice was performed by i.p. injection of 6.25 mg/kg antibody reconstituted in normal saline.

Tnfr1/2 Gene Knockout Mice

TNF receptor knockout mice were purchased from the Jackson Laboratory: *Tnfr1/2*$^{-/-}$ (Tnfrsf1a^{tm1Imx}; stock number 003243). Wild-type controls were used as follows: C57BL/6J; stock number 000664 and 129S F2 hybrid. Breeding of homozygous mice was performed in the animal facility of Massachusetts Eye and Ear Infirmary. Burns were performed as described above, and retinas were isolated and analyzed using flow cytometry and immunohistochemistry. Genotyping was performed to validate TNF receptor deletion.

Statistical Analysis

Results were analyzed with the SPSS version 17.0 (Statistical Package for the Social Sciences Inc., Chicago, IL). The normality of continuous variables was assessed using the Kolmogorov-Smirnov test. Quantitative variables were expressed as means ± SEM, and qualitative variables were expressed as frequencies and percentages. The Mann-Whitney test was used to assess differences between the groups. All tests were two tailed, and statistical significance was determined at $P < 0.05$. Bonferroni correction was applied as appropriate for multiple comparisons.

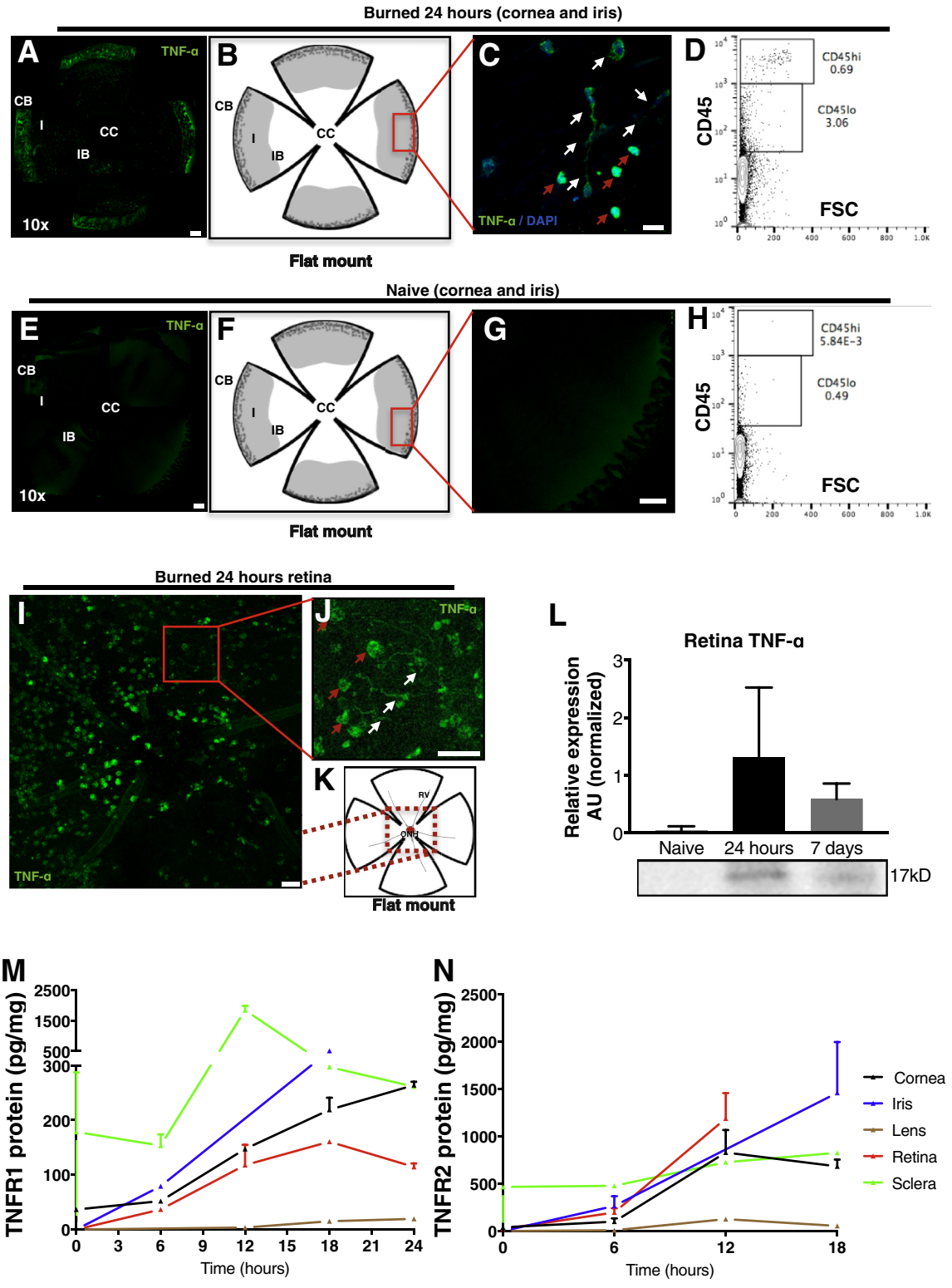

Figure 3 TNF expression in the cornea, iris, and retina after ocular alkali burn. TNF-α expression in the iris is up-regulated 24 hours after the burn (**A**–**C**) with concomitant increase in CD45 expression (**D**) as compared to naive nonburned eyes (**E**–**H**). **C:** TNF-α–secreting cells in the iris are mainly amoeboid (**red arrows**) and dendritiform (**white arrows**) cells. Amoeboid cells have stronger TNF-α expression as compared to dendritiform cells. **I:** TNF-α expression is also up-regulated in the retina at 24 hours after burn. **I**–**K:** A significant number of TNF-α–expressing cells are found in the vicinity of the optic nerve head and these cells are amoeboid (**red arrows**) and dendritiform (**white arrows**). **L:** TNF-α expression up-regulation in the retina is confirmed with immunoblotting, which shows elevation of TNF-α expression at 24 hours and 7 days after the burn. **M** and **N:** Tnf-r1 and r2 expression is up-regulated in the cornea, iris, and retina after corneal burn, but not in the sclera or lens. Data are expressed as means ± SD (**L**). $n = 9$ (**L**). Scale bars: 200 μm (**A**, **C**, **E**, and **G**); 25 μm (**I** and **J**). AU, arbitrary unit; CB, ciliary body; CC, central cornea; FSC, forward scatter; I, iris; IB, iris boarder; ONH, optic nerve head; RV, retinal vessel.

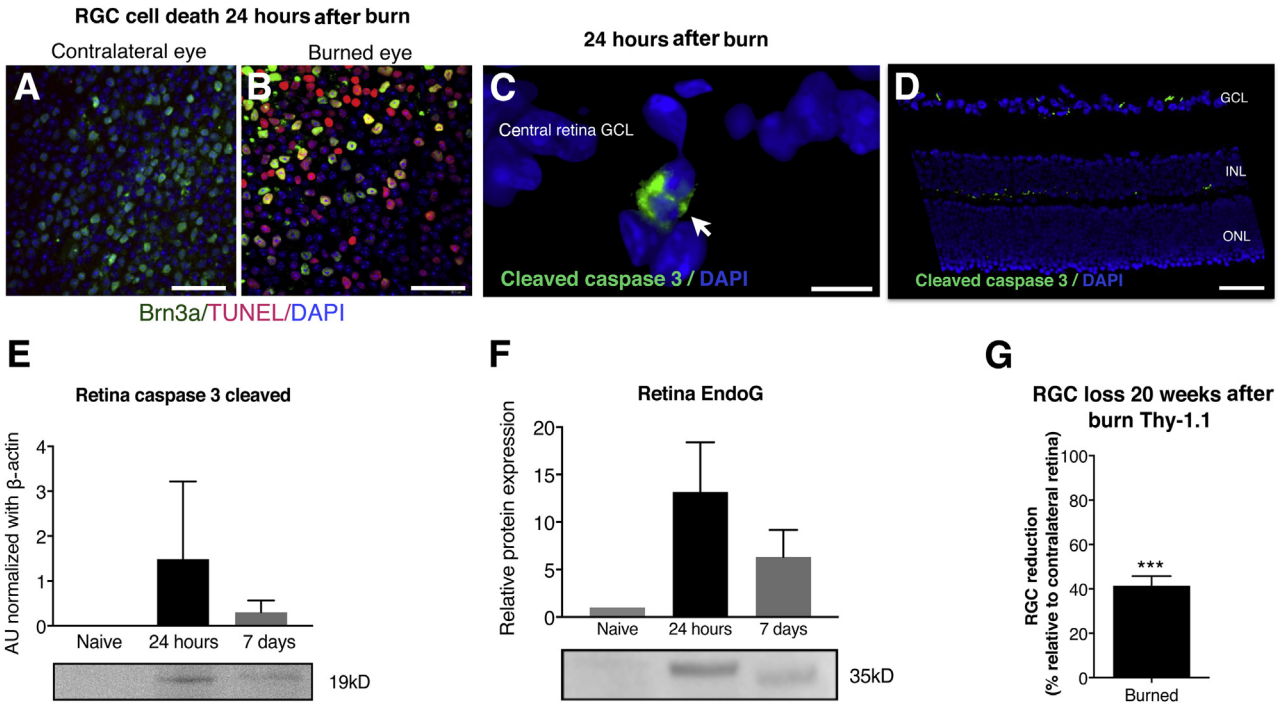

Figure 4 Retinal damage after ocular alkali burn. **A** and **B:** Alkali burn causes acute retinal ganglion cell (RGC) death 24 hours after the burn, as suggested by Brn3a (green) and TUNEL (red) staining in retinal flat mounts. Cleaved caspase-3 is predominantly expressed in the ganglion cell layer (**white arrow**, **C**) and in the inner nuclear layers 24 hours after the burn (**D**). **E:** Cleaved caspase-3 is up-regulated in the retina 24 hours after the burn and remains increased at 7 days. Naive nonburned eyes show no expression of cleaved caspase-3. **F:** Endonuclease G (EndoG) protein is also up-regulated 24 hours and 7 days after the burn. **G:** Alkali burn results in significant RGC loss by week 30, approximately 40% as compared to contralateral nonburned control eyes. Data are expressed as means ± SD (**E**–**G**). $n = 6$ (**E** and **F**). $^{***}P < 0.001$. Scale bars: 40 μm (**A** and **B**); 10 μm (**C**); 50 μm (**D**). AU, arbitrary unit; ONL, outer nuclear layer.

Results

Alkali Burn to the Cornea Causes Direct Physical Damage to the Anterior But Not to the Posterior Structures

In vivo pH, oxygen, and redox measurements were performed in mice and rabbits after corneal alkali burn with 1 and 2 mol/L sodium hydroxide, respectively. The use of two different animal models aimed to assess the effect of ocular size on retinal damage after corneal alkali burn and the ability of the mouse alkali burn model to replicate the dynamics of larger eyes. A micro pH probe was implanted in the aqueous humor (AH) of the anterior chamber (AC) of mice through a corneal-limbal incision before the burn and remained in place after the burn (Figure 1A). At 40 seconds after the burn, the pH in the AC of mice increased from 7.4 to 11.4 (Figure 1, B and C). The pH returned to physiological levels at 45 minutes after the burn (Figure 1C). Alkali diffusion posteriorly was also investigated by implanting a pH sensor in the vitreous through a pars-plana scleral incision (Figure 1D). Sequential measurements in separate mice covering a period of 26 hours after the burn showed no evidence of pH elevation in the vitreous, with the pH in the vitreous remaining constant at 7.3 (Figure 1, E and F).

pH measurements were also performed *in vivo* in rabbits after corneal surface burn with alkali. A micro pH probe was implanted in the anterior chamber through a corneal-limbal incision before the burn (Figure 1, G and H). Sodium hydroxide (2 mol/L) was applied to the central cornea using an 8-mm diameter filter paper for 60 seconds, followed by saline irrigation for 15 minutes. The pH in the AC was 7.3 before the burn and increased to 11.4 within 60 seconds after the burn (Figure 1I). The pH gradually decreased to normal levels (pH 7.3) over 180 minutes and stabilized below the preinjury levels (pH 6.9) between 180 and 230 minutes after the burn (Figure 1I). This slightly acidic environment was attributed to the anterior chamber tissue injury.

To investigate the possibility of alkali diffusion to the retina of rabbits via the uveoscleral outflow, pH in the suprachoroidal space was also measured (Figure 1J). The probe was implanted via a pars-plana scleral incision and advanced posteriorly in the suprachoroidal space to reach an area adjacent to the optic nerve, where it was left *in situ* for 25 hours (Figure 1K). The animals remained anesthetized throughout the experiment and were euthanized at the end of the experiment. No pH elevation was measured in the suprachoroidal space up to 25 hours after burn (Figure 1L). Conversely, a gradual decrease in pH, from 7.4 to 7.2 (Figure 1L), was noted and attributed to surgical trauma.

Oxygen levels were also measured in the anterior and posterior segments of mouse and rabbit eyes using miniaturized implantable sensors. Implantation of the sensor was performed as previously described in the pH experiments.

AH oxygen level in mice exhibited significant reduction within 30 seconds after the burn from 178 ± 8.5 μmol/L (170 to 190 μmol/L) to 44 ± 24 μmol/L (10 to 65 μmol/L), $P < 0.001$ ($n = 4$). AH oxygen level returned to normal 30 minutes after the burn (Supplemental Figure S1A). Vitreous oxygen was not affected by the burn and remained constant before and after the burn, with oxygen level before of 36 ± 8 μmol/L (30 to 41 μmol/L) after the burn of 40 ± 3 μmol/L (38 to 42 μmol/L), $P = 0.656$ ($n = 3$) (Supplemental Figure S1B). Likewise, redox potential in the AH of mice exhibited reduction within 30 seconds after the burn from 240 mV to −10 mV and then returned to near

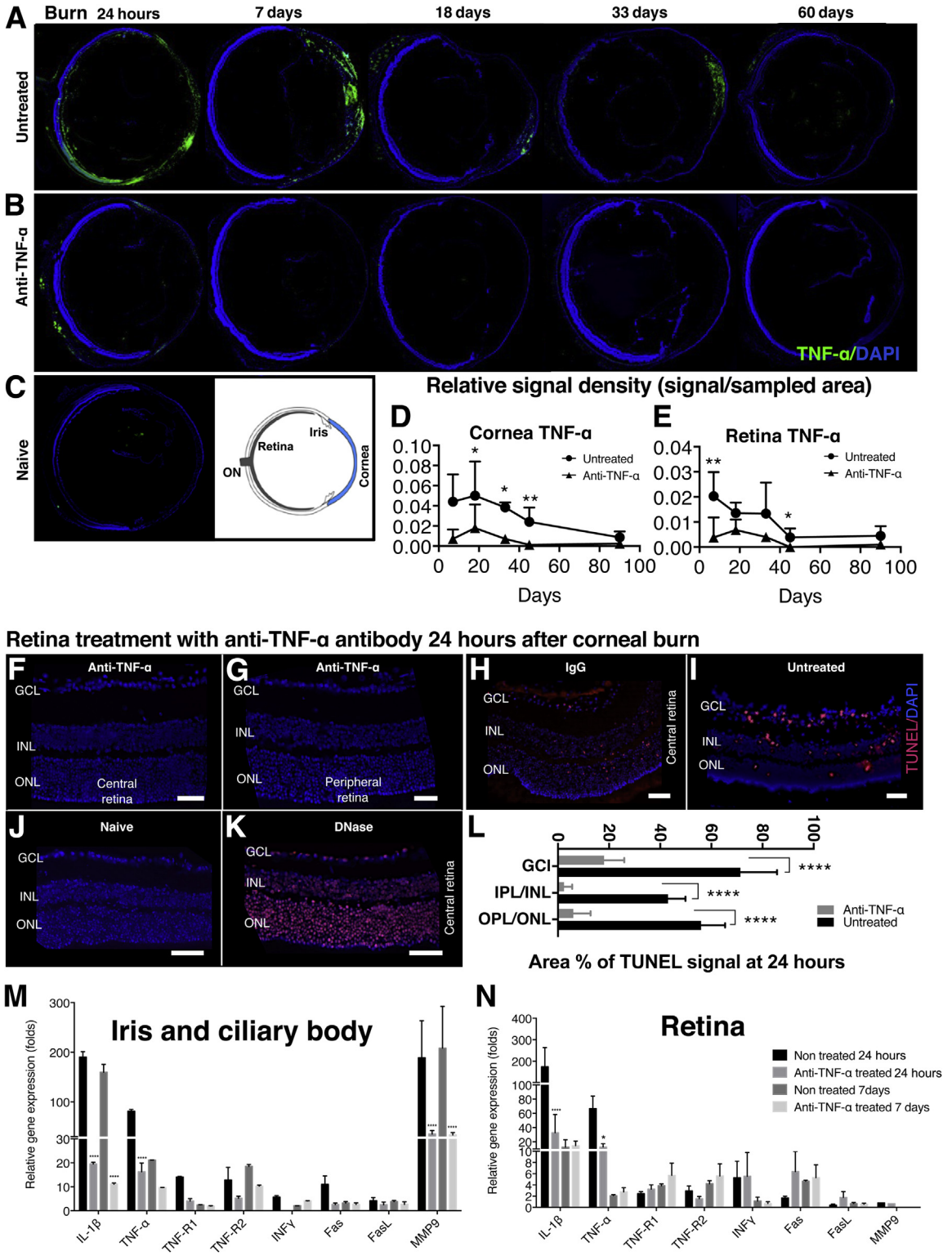

normal level 95 minutes after the burn (Supplemental Figure S1C). However, vitreous redox state was not affected by the burn and remained constant at 280 mV before and after the burn (Supplemental Figure S1D). In addition, the intraocular pressure of the eye was not affected by the burn at 24 hours (Supplemental Figure S1E).

Likewise, rabbit eyes exhibited similar oxygen reduction in the AC, with oxygen descending from 170 to 5 μmol/L 3 minutes after the burn and then returning to normal level 30 minutes after the burn (Supplemental Figure S1F). Conversely, vitreous oxygen level remained constant at 50 μmol/L after the burn (Supplemental Figure S1G). Intracameral pressure measurements showed no significant IOP elevation during the first 24 hours of the burn (Supplemental Figure S1H).

Corneal Alkali Burn Causes Anterior Uveal Inflammation that Propagates Posteriorly to the Retina

At 24 hours after the burn, $CD45^+$ cell numbers increased in the iris and ciliary body (Figure 2A). Of the $CD45^+$ cells, 52% were $Ly6C^+$ $Ly6G^+$ and only 10% were either $Ly6C^+$ or $Ly6G^+$. Of the $CD45^+$ $Ly6C^+$ $Ly6G^+$ cells, 28% were $CD11b^+$ MHC-II^+ and 49% $CD11b^+$ MHC-II^-. $Ly6G^+$ $Ly6C^-$ had no MHC-II expression, whereas 9% of the $Ly6G^-$ $Ly6C^+$ expressed $CD11b^+$ MHC-II^+ markers. However, a significant number (11%) of MHC-II^+ expressing cells were $CD11b^-$. In nonburned eyes, the number of $CD45^+$ $Ly6C^+$ $Ly6G^+$ cells was low (Figure 2B).

Corneal alkali burn caused significant up-regulation of inflammatory cytokine mRNA in the iris and ciliary body as compared to naive controls. *Tnfa*, *Il1b*, *Tnfr1*, *Tnfr2*, *Fas*, and *Mmp9* gene expression levels were significantly up-regulated 24 hours after the burn [IL-1β, 190-fold; TNF-α, 90-fold; TNF-R1, 13-fold; TNF-R2, 12-fold; interferon (INF)-γ, fivefold; Fas, 11-fold; matrix metalloproteinase (MMP) 9, 200-fold; normalized to naive control]. FasL was not affected by the burn. Seven days after the burn, TNF-α, IL-1β, TNF-R2, and MMP9 mRNA levels remained elevated, whereas TNF-R1, INF-γ, and Fas returned to normal (Figure 2C). Likewise, retinal inflammatory cytokine mRNAs were also up-regulated. TNF-α, IL-1β, and INF-γ levels were increased 24 hours after the burn (IL-1β, 200-fold; TNF-α, 50-fold; INF-γ, sixfold; normalized to naive control) and with the exception of IL-1β returned to normal levels 7 days after the burn (Figure 2D). *Tnfr1* and *r2* gene expression was marginally increased 7 days after the burn, whereas *Mmp9* expression in the retina remained unchanged at both time points after burn.

TNF-α expression in the iris, ciliary body, and retina was evaluated by confocal microscopy. At 24 hours after the burn, the iris and ciliary body showed a marked up-regulation of TNF-α (Figure 3, A–C), expressed by amoeboid and dendritiform cells (Figure 3C). A concomitant increase in $CD45^+$ cells was also noted (Figure 3D). Conversely, naive nonburned eyes showed no TNF-α expression in the iris (Figure 3, E–G) and minimal expression of $CD45^+$ cells (Figure 3H). Retinal TNF-α expression was also up-regulated at 24 hours after the burn, with most TNF-α–expressing cells residing around the optic nerve head and having amoeboid and dendritiform appearance (Figure 3, I–K). Retinal TNF-α up-regulation 24 hours and 7 days after the burn was confirmed with immunoblot (Figure 3L). TNF-R1 and TNF-R2 protein expression was up-regulated in the cornea, iris, and retina within 6 hours after the burn, reaching a plateau by 12 to 18 hours after the burn (Figure 3, M and N). Iris TNF-R1 and R2 expression remained elevated 18 hours after the burn, but the lens and sclera showed no marked change in TNF-R1 and TNF-R2 expression (Figure 3, M and N).

Corneal Alkali Burn Causes RGC Death

To evaluate the extent of RGC death after corneal alkali burn, mouse retinas were flat mounted and evaluated with Brn3a and TUNEL assays. At 24 hours after the burn, $Brn3a^+$ cells showed increased numbers of $TUNEL^+$ nuclei (Figure 4, A and B). As shown previously (Supplemental Figure S1E), RGC damage was not attributable to IOP elevation ($P = 0.401$) but rather involved up-regulation of caspase 3 (Figure 4, C–E) and endonuclease G (Figure 4F).

Figure 5 Ocular protection with anti–TNF-α treatment. **A–C:** Ocular tissue sections (10 μm thick) of mice burned with 1 mol/L sodium hydroxide followed by copious irrigation with saline solution for 15 minutes. **A:** TNF-α expression (green) is elevated in all intraocular tissues 24 hours after the burn, with diffuse anterior uveal expression persisting up to 7 days after the burn. **B:** Conversely, anti–TNF-α–treated mice (infliximab, 6.25 mg/kg), administered immediately after irrigation, exhibit reduced TNF-α (green) expression in all ocular tissues. **C:** No TNF-α expression is present in the eyes of naive control mice. **D** and **E:** Quantification of TNF-α fluorescence shows up-regulation in the cornea and retina 24 hours after the burn, which is sustained for 45 days and then gradually decreases. TNF-α expression is undetectable in the corneal and retina of anti–TNF-α–treated mice 45 days after the burn. Anti–TNF-α treatment inhibits central (**F**) and peripheral (**G**) retinal cell apoptosis, as shown using TUNEL assay (red) 24 hours after corneal burn. **H:** Systemic administration of 6.25 mg/kg IgG isotype control does not inhibit retinal cell apoptosis 24 hours after corneal burn. **I:** Untreated eyes have elevated TUNEL expression in the retina 24 hours after corneal burn. **J:** Naive control tissue has no TUNEL signal. **K:** Ten-minute DNase treatment of naïve tissue causes TUNEL-positive expression in cells. **L:** Corneal alkali burn causes significant apoptosis in the retinal ganglion cell layer (GCL), inner nuclear layer (INL)/inner plexiform cell layer (IPL), and outer nuclear layer (ONL)/outer plexiform cell layer (OPL) 24 hours after the burn. Prompt TNF-α inhibition with anti–TNF-α antibody significantly reduces the relative TUNEL expression in all retinal layers ($P < 0.0001$). Anti–TNF-α treatment suppresses TNF-α, TNF-R1, TNF-R2, IL-1β, Fas, and MMP9 expression in the iris and ciliary body (**M**) and reduces TNF-α and IL-1β expression in the retina (**N**). Anti–TNF-α therapy causes a moderate (nonsignificant) increase in TNF-R1, TNF-R2, Fas, and FasL expression in the retina but significantly suppresses IL-1β expression in the retina. Data are expressed as means ± SD (**D**, **E**, **L–N**). $n = 10$ (**D** and **E**). $^*P < 0.05$, $^{**}P < 0.01$, and $^{****}P < 0.0001$ compared to untreated eyes. Scale bar = 50 μm (**F–K**).

Both pathways were up-regulated in the retina 24 hours and 7 days after the burn. Cleaved caspase-3 was primarily expressed in the ganglion cell layer (GCL) and on the interface between the inner nuclear layer (INL) and outer plexiform layer (Figure 4, C and D) 24 hours after the burn. Retinal caspase 3 was up-regulated at 24 hours after the burn and remained elevated 7 days after the burn (Figure 4E). Endonuclease G was up-regulated in the retina 24 hours after the burn and remained elevated 7 days after the burn (Figure 4F). In mice, retinal inflammation and cell apoptosis led to a significant 40% ($P < 0.001$) reduction in the number of RGCs in burned eyes, as compared to non-burned contralateral eyes (Figure 4G).

Likewise, corneal alkali burn in rabbits caused diffuse ocular cell apoptosis (Supplemental Figure S2). As expected, damage to the cornea and uvea developed within 10 hours of the burn (Supplemental Figure S2, A–F). Within the same time frame, the peripheral retina showed early damage in all retinal layers and the central retina showed damage primarily in the GCL (Supplemental Figure S2, G–I). Significant $TUNEL^+$ staining was noted in all retinal layers 2 weeks after the burn (Supplemental Figure S2J). No $TUNEL^+$ expression was found in control untreated rabbit ocular tissues (Supplemental Figure S2, K–N). Three months after the burn, RGC numbers and optic nerve axons of rabbit eyes significantly declined to 40% ($P = 0.036$) and 38% ($P < 0.001$), respectively (Supplemental Figure S3, A–F), as compared to measurements performed in the contralateral, nonburned eyes. However, systemic anti–TNF-α administered 15 minutes after the burn significantly reduced RGC loss ($P = 0.008$) measured at 6 to 9 months after the burn (Supplemental Figure S3, G–I).

Prompt Anti–TNF-α Therapy Suppresses Inflammation and Protects the Retina in Alkali Cornea Burn

Emergency irrigation with buffers, such as Cederroth (Cederroth AB, Upplands Väsby, Sweden) or saline solution is the standard of care in the acute management of ocular chemical burns.[19,20] Irrigation with Cederroth or normal saline solution was performed immediately after experimental burns in mice eyes for 15 minutes (standard emergency protocol). Cederroth irrigation had no effect in reducing TUNEL expression in the eye (Supplemental Figure S4, A and B). Despite irrigation, alkali burn caused conspicuous TUNEL expression in the cornea, iris, and peripheral retina. Cells in the GCL exhibited the most profound $TUNEL^+$ expression compared to the other retinal cell layers. No $TUNEL^+$ expression was present in control untreated eyes (Supplemental Figure S4C). Likewise, high-dose systemic corticosteroid (dexamethasone, 120 mg/kg) administered to mice 15 minutes after the burn provided limited protection to the retina, as evident by $TUNEL^+$ labeling (Supplemental Figure S4, D and E).

To explore the protective effect of anti–TNF-α therapy in ocular alkali burns, a single dose of anti–TNF-α antibody (infliximab, 6.25 mg/kg) was administered i.p. immediately after the burn. Although untreated mice had a sustained increase in corneal and retinal TNF-α expression for 45 days as compared to naïve controls, mice treated with infliximab had significantly lower TNF-α expression in all ocular tissues (Figure 5, A–E). At 24 hours, uveal TNF-α expression in untreated mice was diffuse, and persisted in the anterior uvea up to 7 days after burn (Figure 5A). Anti–TNF-α treatment caused a reduction in TNF-α expression in the uvea (Figure 5B) and protected the retina from apoptosis, as evident by reduced $TUNEL^+$ labeling (Figure 5, F and G). Systemic administration of isotype IgG control (6.25 mg/kg i.p.) (Figure 5H) or no treatment (Figure 5I) did not prevent retinal cell apoptosis. Naive, nonburned eyes were used for negative controls (Figure 5J) and DNase-treated eyes as positive control (Figure 5K). Quantification of retinal cell apoptosis 24 hours after the burn showed increased percentage of $TUNEL^+$ signal in the GCL, INL/inner plexiform layer, and outer nuclear layer/outer plexiform layer as compared to mice that received anti–TNF-α therapy [difference in TUNEL signal between untreated and anti–TNF-α–treated mice: GCL ($P = 0.0006$), INL/outer plexiform layer ($P < 0.0001$), and outer nuclear layer/outer plexiform layer ($P = 0.0001$)] (Figure 5L). In addition, anti–TNF-α treatment suppressed the mRNA levels of TNF-α (by 70-fold; $P < 0.005$), IL-1β (170-fold; $P < 0.0001$), and MMP9 (165-fold; $P < 0.0001$) in the iris 24 hours after alkali burn (Figure 5M). Iris TNF-R1 and TNF-R2, Fas, and INF-γ gene expression levels at 24 hours were also suppressed by infliximab treatment. At 7 days after burn, anti–TNF-α treatment suppressed iris/ciliary body levels of IL-1β, TNF-α, TNF-R2, and MMP9 mRNA by 160-, 10-, 10-, and 180-fold, respectively (Figure 5M).

Twenty-four hours after the burn, anti–TNF-α treatment suppressed retinal TNF-α and IL-1β mRNA levels by 40-fold ($P < 0.05$) and 150-fold ($P < 0.001$), respectively (Figure 5N). Anti–TNF-α treatment increased Fas and FasL mRNA levels marginally and had no significant effect on retinal INF-γ and MMP9 mRNA levels. At 7 days after the burn, regardless of the treatment, retinal TNF-α, INF-γ, FasL, and MMP9 mRNA levels returned to normal levels (compared to naive control), whereas IL-1β and Fas remained elevated. Paradoxically, retinal TNF-R1 and TNF-R2 mRNA levels increased sixfold with the anti–TNF-α treatment, but this change was not statistically significant ($P > 0.05$) (Figure 5N).

TNF-α Signaling Blockade Inhibits the Activation of Inflammatory Cells and Subsequent RGC Apoptosis

To study the role of TNF system signaling in retina damage after corneal alkali burn, TNF receptor 1 and 2 double knockout ($Tnfr1/2^{-/-}$) mice on a C57BL/6J background were studied in comparison to anti–TNF-α–treated wild-type mice (C57BL/6J). $Tnfr1/2^{-/-}$ mice have no ocular phenotype (Jackson Laboratory data sheet). $CD45^+$ cell

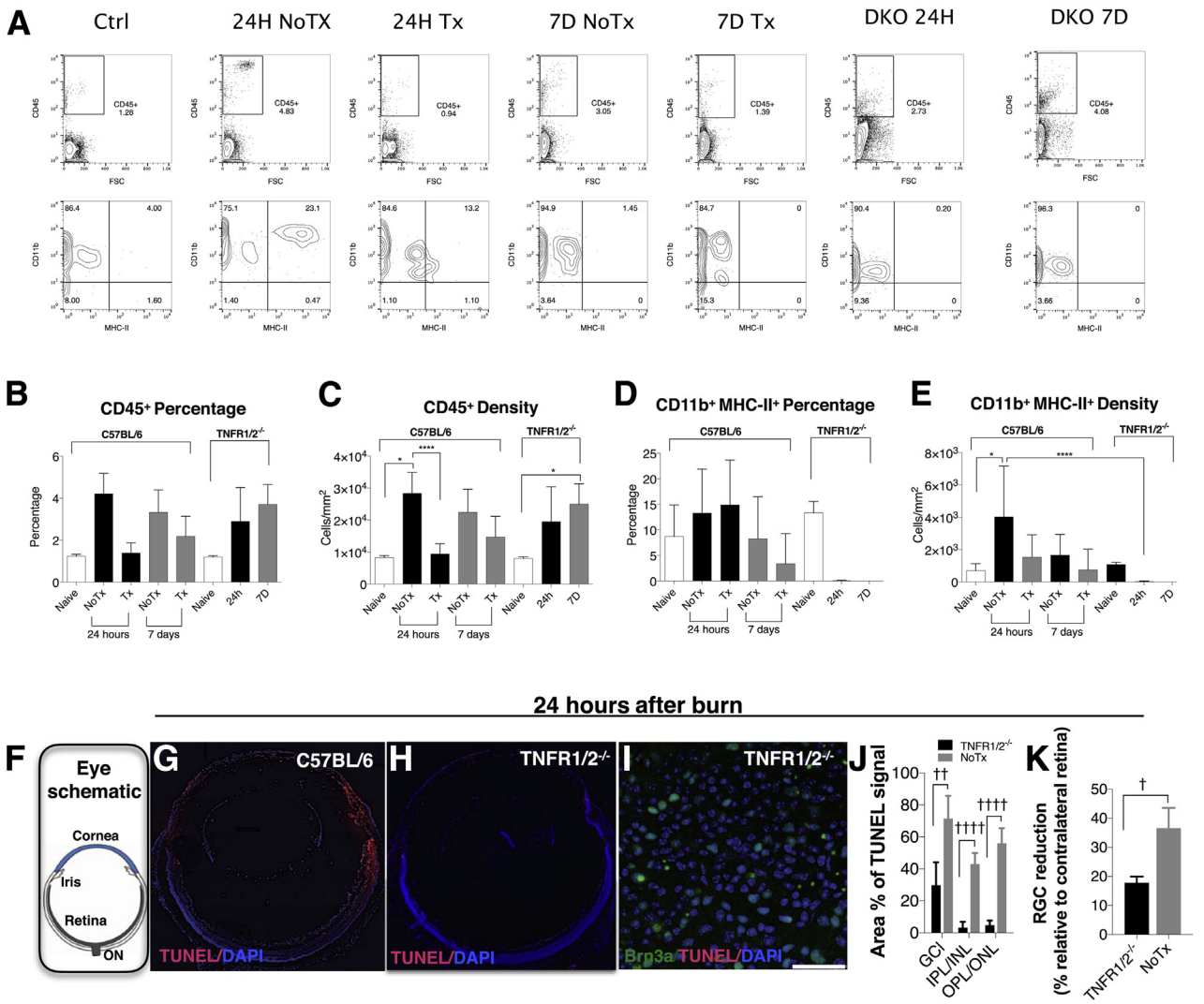

Figure 6 The role of TNF system in inflammation and retinal damage. The role of TNF signaling in retinal damage was investigated using anti—TNF-α monoclonal antibody and TNF-R1/2 knock out mice. **A:** Representative flow cytometry data. Quantification of $CD45^+$ cell expression in the retina. Corneal alkali burn causes up-regulation of CD45 expression in the retina of wild-type mice at 24 hours (**B** and **C**) and MHC-II expression up-regulation by $CD45^+$ $CD11b^+$ cells (**D** and **E**). Prompt anti—TNF-α treatment significantly reduces $CD45^+$ cell expression in the retina ($P = 0.028$) at 24 hours and suppresses MHC-II expression 24 hours and 7 days after the burn. *Tnfr1/2* gene deletion has no significant effect in $CD45^+$ cell infiltration into the retina (**B** and **C**) but significantly suppresses MHC-II expression from $CD45^+$ $CD11b^+$ cells ($P = 0.042$) at 24 hours (**D** and **E**). **F:** Schematic showing the orientation of the tissue in panels **G** and **H**. *Tnfr1/r2*$^{-/-}$ mice demonstrate reduced cell apoptosis (red) in the eye (**G**—**I**) and in the GCL, after corneal alkali burn (**H**). **J:** Deletion of *Tnfr1/2* significantly reduces the percentage of $TUNEL^+$ signal at 24 hours in the GCL ($P = 0.002$), INP/INL ($P = 0.0001$), and outer plexiform layer (OPL)/outer nuclear layer (ONL) ($P = 0.0001$), as compared to untreated C57BL/6 mice. **K:** Likewise, deletion of Tnfr1/2 significantly reduces RGC loss at 7 days, as compared to untreated mice ($P = 0.024$). Data are expressed as means ± SD (**B**—**E**, **J**, **K**). $^*P < 0.05$ (Dunnett's post hoc test; compared to naive), $^{****}P < 0.05$ Tuckey's post hoc (compared to untreated) (C and E); $^{\dagger}P < 0.05$, $^{\dagger\dagger}P < 0.01$, and $^{\dagger\dagger\dagger\dagger}P < 0.0001$ (independent *t*-test) (**J** and **K**). Scale bar = 40 μm (**I**). DKO, double receptor knockout (Tnfr1/2$^{-/-}$); NoTx, untreated; Tx, anti—TNF-α treatment.

activation in these mice after burn was assessed by MHC-II expression in $CD45^+$ $CD11b^+$ subpopulations, and anti—TNF-α treatment was used as a treatment control. Corneal burn led to a significant ($P = 0.006$) increase in CD45 expression in the retina of wild-type animals (Figure 6, A—C), which was associated with marked up-regulation of MHC-II expression ($P = 0.047$) (Figure 6, A, D, and E). Corneal alkali burns in Tnfr1/2$^{-/-}$ mice increased CD45 expression to significant levels 7 days after the burn ($P = 0.024$) (Figure 6, A—C), but also led to abrogation of MHC-II expression 24 hours and 7 days after burn (Figure 6, A, D, and E). Anti—TNF-α treatment did not cause significant reduction in CD45 expression in the retina 24 hours after the burn in wild-type animals but led to marked reduction in MHC-II expression from $CD45^+$ $CD11b^+$ cells as compared to wild-type burned mice (Figure 6, D and E). MHC-II suppression was more evident in Tnfr1/2$^{-/-}$ mice than in wild-type mice treated with anti—TNF-α (Figure 6, D and E). Tnfr1/2 gene deletion led to a significant reduction in retinal cell apoptosis, as

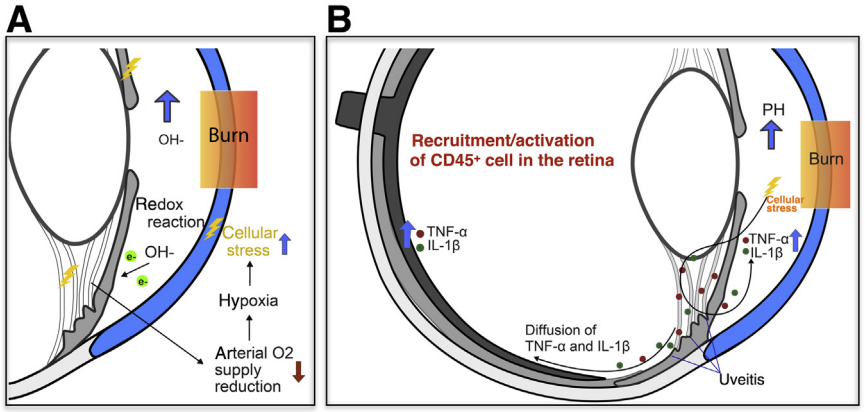

Figure 7 A proposed model for retinal damage in ocular alkali burns. **A:** Alkali burn to the cornea increases hydroxyl ions in the aqueous humor (AH). This leads to AH reduction and cell oxidation. In turn, this causes reduction in oxygen supply by iris vessels, cellular stress, and up-regulation of inflammatory mediators in the uvea. **B:** TNF-α and IL-1β are up-regulated in the iris and retina and cause infiltration and activation of immune cells, and retinal inflammation. Up-regulation of TNF-α in the retina activates apoptotic signals, such as caspase 3 and endonuclease G, which results in cell apoptosis and optic nerve degeneration.

demonstrated by reduced TUNEL$^+$ signal in all retinal layers at 24 hours after the burn (Figure 6, G and H). Tnfr1/2 gene deletion caused significant reduction in relative TUNEL expression 24 hours after the burn in the GCL ($P = 0.002$), inner plexiform cell layer/inner nuclear layer ($P = 0.0001$), and outer plexiform layer/outer nuclear layer ($P = 0.0001$), as compared to untreated C57BL/6 mice (Figure 6, F–J). Likewise, Tnfr1/2 gene deletion reduced RGC loss ($P = 0.024$) 7 days after the burn (Figure 6K).

Discussion

Alkali burns of the anterior segment can cause damage not only to the cornea but also result in widespread damage to the retina with later optic nerve pallor and glaucomatous cupping developing in severe cases.[21] This was recently documented in a clinical study of 28 patient eyes with corneal blindness from alkali burns, who subsequently underwent implantation of a Boston keratoprosthesis, allowing a clear view of the retina.[8] Most of these patients had glaucoma before Boston keratoprosthesis implantation or exhibited de novo glaucoma after Boston keratoprosthesis implantation. These eyes with prior alkali burns demonstrated accelerated progression compared to nonburned Boston keratoprosthesis patients, despite aggressive anti-glaucoma medication and surgery.[22]

Until now, the mechanism of posterior segment injury after ocular surface burn has been obscure. To date, the few published studies have suggested that retinal and optic nerve damage were likely because of alkali diffusion posteriorly, or to IOP elevation.[21,23–25] In a more recent investigation, IL-1 and IL-6 up-regulation were shown in mice retinas 3 days after an experimental burn, which the authors attributed to a putative diffusion of alkali to the posterior segment, but without direct experimental evidence.[26] In our prior pilot study, pH measurements in rabbit eyes after alkali burns cast doubt on the diffusion of alkali to the retina after corneal burn.[11]

Our current study found no change in pH in the vitreous or suprachoroidal space during the first 24 hours after burn in either mice or rabbit eyes. *In vivo* measurements in living animals confirmed that the alkaline agent does not reach the retina. Instead, the present study suggests that the anterior segment (cornea, iris, ciliary body, and lens) experiences direct pH injury with dramatic hypoxia and redox potential reduction that lead to severe inflammation affecting the posterior segment despite pH, oxygen, and redox potential in the vitreous remaining unaffected. pH normalization in the AC of rabbits was four times slower than in mice eyes. This was attributed to ocular volume differences. More important, the pH of the AH in both animals reached the same levels within a minute and normalization was gradual and not affected or accelerated by copious irrigation with saline solution. This suggests that pH normalization in the AC occurs through aqueous humor replenishment, and it remains unaffected by ocular irrigation after alkaline burn.

We identified profound up-regulation for TNF-α, TNFR-1, TNFR-2, IL-1β, and MMP9 in iris and ciliary body after corneal burn. TNF-α and IL-1β are known to contribute to the pathogenesis of noninfectious anterior uveitis,[27] and uveal inflammation itself causes further up-regulation of *Tnfa* gene expression as an inflammation-amplifying, positive feedback loop.[28–32] Uveal inflammation causes release of proinflammatory cytokine into the aqueous humor,[33,34] which is likely to diffuse posteriorly and cause retina inflammation, blood retinal barrier disruption, infiltration of immune cells from the blood, and activation of tissue resident immune cells. Alternatively, synaptic signaling via Müller cells may trigger rapid cytokine release in the retina secondary to anterior segment inflammation.[35–37] In either case, induced cellular stress is expected to result in the release of proinflammatory cytokines in the eye.[28–32] The increase in cell apoptosis in the INL and outer nuclear layer of the midperipheral retina in mice and rabbits was attributed to the pH elevation in the AC that caused severe uveal inflammation, especially in the iris and ciliary body (Figure 7, Supplemental Figure S2, G and J, and Supplemental Figure S4, A and B).

The importance of TNF activation was shown by the fact that both neutralizing antibody and gene deletion of the TNF-α receptors resulted in marked suppression of

inflammation in the iris and retina, and inhibition of RGC apoptosis. TNF-α blockade also led to significant IL-1β suppression, consistent with TNF-α acting upstream of IL-1β expression.[38] On the other hand, generic immunosuppression with systemic dexamethasone had a limited protective effect on the retina, underlining the therapeutic importance of targeted immunomodulation. The lack of effect on $CD45^+$ cells in the $Tnfr1/2^{-/-}$ animals as compared to infliximab-treated mice suggests that either TNF acts partially through noncanonical receptors or acute Tnf neutralization is more beneficial or different when compared to global and sustained absence of Tnfr1/2. This may be attributed to compensatory mechanisms that occur when a pathway is permanently deleted, as in knockout mice. In addition, infliximab binding to receptor-bound Tnf-α can cause cell lysis. This can result in subsequent demise of $CD45^+$ cell in wild-type mice but not in knockout mice that lack the receptor.[39,40] Despite the observed differences, both $Tnfr1/2^{-/-}$ and infliximab treatment provided marked suppression of MHC-II expression of $CD45^+$ $CD11b^+$ cells, which should reduce both innate and adaptive immune system activation after burn injury.

In conclusion, alkali injury to the cornea leads to profound pH, oxygen, and redox potential insult to the anterior eye structures but not to the posterior segment. Massive inflammation from the direct injured anterior structures causes recruitment and activation of immune cells in the retina and subsequent damage of the inner and outer retina (Figure 7). IOP elevation seems to be an independent factor for retinal damage. Because both small (mice) and large (rabbit) animal eyes appear to respond similarly to ocular alkali injury and anti−TNF-α treatment, with similar patterns of retinal and optic nerve changes,[41] one can speculate that similar responses may likely occur in the human eye as well. Our study demonstrates a homeostatic link between the anterior and posterior segments of the eye and the role for the uvea in connecting these compartments. Prompt TNF-α blockade (using intravenous antibodies or other TNF-neutralizing agents) is a promising adjunct to the current therapeutic modalities for alkali burns and may help improve the clinical outcomes for human patients experiencing severe burns.

Supplemental Data

Supplemental material for this article can be found at *http://dx.doi.org/10.1016/j.ajpath.2017.02.005*.

References

1. McCulley JP: Chemical injuries. Edited by Smolin G, Thoft RA. In The Cornea: Scientific Foundations and Clinical Practice. ed 2. Philadelphia, PA: Lippincott Williams & Wilkins, 1987. pp. 527−542
2. Wagoner MD: Chemical injuries of the eye: current concepts in pathophysiology and therapy. Surv Ophthalmol 1997, 41:275−313
3. Schrage NF, Langefeld S, Zschocke J, Kuckelkorn R, Redbrake C, Reim M: Eye burns: an emergency and continuing problem. Burns 2000, 26:689−699
4. Pfister RR: Chemical trauma. Edited by Foster CS, Azar DT, Dohlman CH. In Smolin and Thoft's The Cornea: Scientific Foundations and Clinical Practice. ed 4. Philadelphia, PA: Lippincott Williams & Wilkins, 2005. pp. 781−796
5. Abel R, Binder PS, Polack FM, Kaufman HE: The results of penetrating keratoplasty after chemical burns. Trans Am Acad Ophthalmol Otolaryngol 1975, 79:84−95
6. Fagerholm P, Lisha G: Corneal stem cell grafting after chemical injury. Acta Ophthalmol Scand 1999, 77:165−169
7. Tuft SJ, Shortt AJ: Surgical rehabilitation following severe ocular burns. Eye (Lond) 2009, 23:1966−1971
8. Cade F, Grosskreutz CL, Tauber A, Dohlman CH: Glaucoma in eyes with severe chemical burn, before and after keratoprosthesis. Cornea 2011, 30:1322−1327
9. Miyamoto F, Sotozono C, Ikeda T, Kinoshita S: Retinal cytokine response in mouse alkali-burned eye. Ophthalmic Res 1998, 30:168−171
10. Lin MP, Ekşioğlu Ü, Mudumbai RC, Slabaugh MA, Chen PP: Glaucoma in patients with ocular chemical burns. Am J Ophthalmol 2012, 154:481
11. Cade F, Paschalis EI, Regatieri CV, Vavvas DG, Dana R, Dohlman CH: Alkali burn to the eye: protection using TNF-α inhibition. Cornea 2014, 33:382−389
12. Committee for the Update of the Guide for the Care and Use of Laboratory Animals; National Research Council: Guide for the Care and Use of Laboratory Animals. ed 8. Washington, DC, National Academies Press, 2011
13. Moore LR, Chang SF, Greenstein ET: Urethane-acepromazine: a novel method of administering parenteral anesthesia in the rabbit. Methods Find Exp Clin Pharmacol 1987, 9:711−715
14. Boniello C, Mayr T, Bolivar JM, Nidetzky B: Dual-lifetime referencing (DLR): a powerful method for on-line measurement of internal pH in carrier-bound immobilized biocatalysts. BMC Biotechnol 2012, 12:11
15. Paschalis EI, Chodosh J, Spurr-Michaud S, Cruzat A, Tauber A, Behlau I, Gipson I, Dohlman CH: In vitro and in vivo assessment of titanium surface modification for coloring the backplate of the Boston keratoprosthesis. Invest Ophthalmol Vis Sci 2013, 54:3863−3873
16. Madigan MC, Sadun AA, Rao NS, Dugel PU, Tenhula WN, Gill PS: Tumor necrosis factor-alpha (TNF-alpha)-induced optic neuropathy in rabbits. Neurol Res 1996, 18:176−184
17. Sadun AA, Win PH, Ross-Cisneros FN, Walker SO, Carelli V: Leber's hereditary optic neuropathy differentially affects smaller axons in the optic nerve. Trans Am Ophthalmol Soc 2000, 98:223−232
18. Kimura K, Morita Y, Orita T, Haruta J, Takeji Y, Sonoda K-H: Protection of human corneal epithelial cells from TNF-α-induced disruption of barrier function by rebamipide. Invest Ophthalmol Vis Sci 2013, 54:2572−2760
19. Rihawi S, Frentz M, Schrage NF: Emergency treatment of eye burns: which rinsing solution should we choose? Graefes Arch Clin Exp Ophthalmol 2006, 244:845−854
20. Hamill CE, Bozorg S, Peggy Chang H-Y, Lee H, Sayegh RR, Shukla AN, Chodosh J: Corneal alkali burns: a review of the literature and proposed protocol for evaluation and treatment. Int Ophthalmol Clin 2013, 53:185−194
21. Smith RE, Conway B: Alkali retinopathy. Arch Ophthalmol 1976, 94:81−84
22. Crnej A, Paschalis EI, Salvador-Culla B, Tauber A, Drnovsek-Olup B, Shen LQ, Dohlman CH: Glaucoma progression and role of glaucoma surgery in patients with Boston keratoprosthesis. Cornea 2014, 33:349−354
23. Hughes WF: Alkali burn of the eye. Arch Ophthalmol 1946, 35:423
24. Hughes WF: Alkali burns of the eye. Arch Ophthalmol 1946, 36:189−214

25. Kaplunovich PS, Kalugina MA, Dik GM: [Morphological changes in the choroid and retina in experimental alkali burns of the cornea] Russian. Vestn Oftalmol 1973, 5:39−41
26. Sotozono C, He J, Matsumoto Y, Kita M, Imanishi J, Kinoshita S: Cytokine expression in the alkali-burned cornea. Curr Eye Res 1997, 16:670−676
27. Ooi KG, Galatowicz G, Calder VL, Lightman SL: Cytokines and chemokines in uveitis: is there a correlation with clinical phenotype? Clin Med Res 2006, 4:294−309
28. Helbig H, Hinz JP, Kellner U, Foerster MH: Oxygen in the anterior chamber of the human eye. Ger J Ophthalmol 1993, 2:161−164
29. Chandel NS, Trzyna WC, McClintock DS, Schumacker PT: Role of oxidants in NF-kappa B activation and TNF-alpha gene transcription induced by hypoxia and endotoxin. J Immunol 2000, 165:1013−1021
30. Gupta SC, Hevia D, Patchva S, Park B, Koh W, Aggarwal BB: Upsides and downsides of reactive oxygen species for cancer: the roles of reactive oxygen species in tumorigenesis, prevention, and therapy. Antioxid Redox Signal 2012, 16:1295−1322
31. Reily C, Mitchell T, Chacko BK, Benavides G, Murphy MP, Darley-Usmar V: Mitochondrially targeted compounds and their impact on cellular bioenergetics. Redox Biol 2013, 1:86−93
32. Santo-Domingo J, Wiederkehr A, De Marchi U: Modulation of the matrix redox signaling by mitochondrial Ca(2.). World J Biol Chem 2015, 6:310−323
33. Wakefield D, Lloyd A: The role of cytokines in the pathogenesis of inflammatory eye disease. Cytokine 1992, 4:1−5
34. de Vos AF, van Haren MA, Verhagen C, Hoekzema R, Kijlstra A: Kinetics of intraocular tumor necrosis factor and interleukin-6 in endotoxin-induced uveitis in the rat. Invest Ophthalmol Vis Sci 1994, 35:1100−1106
35. Alberts B, Johnson A, Lewis J, Raff M, Roberts K, Walter P: Molecular Biology of the Cell. ed 4. New York, NY, Garland Science, 2002
36. Bringmann A, Pannicke T, Grosche J, Francke M, Wiedemann P, Skatchkov SN, Osborne NN, Reichenbach A: Müller cells in the healthy and diseased retina. Prog Retin Eye Res 2006, 25: 397−424
37. Reichenbach A, Bringmann A: Müller Cells in the Healthy and Diseased Retina. ed 1. New York, NY, Springer New York, 2010
38. Brennan FM, Jackson A, Chantry D, Maini R: Inhibitory effect of TNFα antibodies on synovial cell interleukin-1 production in rheumatoid arthritis. Lancet 1989, 8657:244−247
39. Siegel SA, Shealy DJ, Nakada MT, Le J, Woulfe DS, Probert L, Kollias G, Ghrayeb J, Vilcek J, Daddona PE: The mouse/human chimeric monoclonal antibody cA2 neutralizes TNF in vitro and protects transgenic mice from cachexia and TNF lethality in vivo. Cytokine 1995, 7:15−25
40. Maini RN, Feldmann M: How does infliximab work in rheumatoid arthritis? Arthritis Res 2002, 4 Suppl 2:S22−S29
41. Zhou C, Robert M-C, Kapoulea V, Lei F, Stagner AM, Jakobiec FA, Dohlman CH, Paschalis EI: Sustained subconjunctival delivery of infliximab protects the cornea and retina following alkali burn to the eye. Invest Ophthalmol Vis Sci 2017, 58:96−105